STRUCTURAL CHEMISTRY

ISSN 2053-2296

Tolerance factor and phase stability of the garnet structure

Zhen Song, Dandan Zhou and Quanlin Liu*

Beijing Key Laboratory for New Energy Materials and Technologies, School of Materials Science and Engineering, University of Science and Technology Beijing, Beijing 100083, People's Republic of China. *Correspondence e-mail: qlliu@ustb.edu.cn

Received 1 July 2019
Accepted 29 August 2019

Edited by H. Shepherd, University of Canterbury, England

Keywords: garnet; tolerance factor; crystal structure; phase stability.

Supporting information: this article has supporting information at journals.iucr.org/c

We introduce a structural descriptor, the tolerance factor, for the prediction and systematic description of the phase stability with the garnet structure. Like the tolerance factor widely adopted for the perovskite structure, it is a compositional parameter derived from the geometrical relationship between multi-type polyhedra in the garnet structure, and the calculation only needs the information of the ionic radius. A survey of the tolerance factor over 130 garnet-type compounds reveals that the data points are scattered in a narrow range. The tolerance factor is helpful in understanding the crystal chemistry of some garnet-type compounds and could serve as a guide for predicting the stability of the garnet phase. The correlation between the tolerance factor and the garnet-phase stability could be utilized by machine learning or high-throughput screening methods in material design and discovery.

1. Introduction

Chemical compositions and crystal structures are central to chemistry and materials science. It is very interesting and useful to predict the phase stability of a specific structure on the basis of composition. As a good example, in perovskite-type compounds, the tolerance factor was first introduced by Goldschmidt in 1926 to describe the phase stability with the ionic radii of the chemical components (Goldschmidt, 1926). Since then, it has been used extensively by researchers in new material discovery and performance improvement in the fields of solar cells (Green *et al.*, 2014; Saliba *et al.*, 2016), ferroelectricity (Itoh *et al.*, 1999; Grinberg *et al.*, 2013), light-emitting diodes (Lin *et al.*, 2018; Cao *et al.*, 2018) and scintillators (Chen *et al.*, 2018). In addition, the tolerance factor makes high-throughput screening applications of perovskites feasible due to the rapid estimation of material properties (Kieslich *et al.*, 2015; Bartel *et al.*, 2019). Therefore, the structural-descriptor-based approach is very important in materials science.

Garnet-based compounds cover a wide range of fascinating properties in magnetism, batteries (Li *et al.*, 2018; Zhang *et al.*, 2018), lasers (Lu *et al.*, 2002), solid-state lighting (Bachmann *et al.*, 2009), displays (Wang *et al.*, 2016) and biomedical usage (Xu *et al.*, 2018). Owing to the unique crystal structure, garnet-based compounds have a large variety of compositional derivatives (Xia & Meijerink, 2017). It is known that the garnet structure, which was originally solved by Menzer (1929), consists of multi-type polyhedra, which are the dodecahedron (A), the octahedron {B} and the tetrahedron [C]. The stoichiometric formula could be written as $(A)_3\{B\}_2[C]_3\langle D\rangle_{12}$. The ionic site preference is mainly determined by the relative ionic size, because the three polyhedra are quite different in size. For example, in $(Y)_3\{Al\}_2[Al]_3\langle O\rangle_{12}$, the dodecahedron

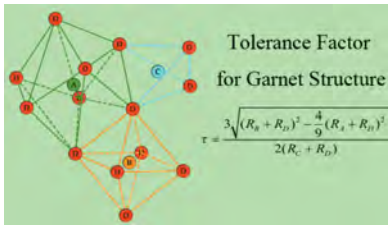

has a volume of about 20 Å^3, while the volumes of the octahedron and tetrahedron only approximate 10 and 3 Å^3, respectively (Song *et al.*, 2018). Therefore, large ions are expected to reside in large polyhedral-volume sites. Rare-earth and alkaline-earth elements generally occupy (A) sites. {B} sites mainly accommodate rare-earth and transition-metal elements. In [C] sites, multi-valent cations have been reported, including V^{5+}/As^{5+}, Si^{4+}/Ge^{4+}, $Al^{3+}/Ga^{3+}/Fe^{3+}$ and Li^{+}. However, the garnet structure is quite flexible, in that larger cations could enter smaller polyhedra, such as the antisite defect formed by Y replacing Al (Muñoz-García *et al.*, 2009, 2012), or the preferential occupancy of Ga in the tetrahedron rather than the octahedron (Laguta *et al.*, 2016). In these cases, the electronic configuration may play an important role (Geller, 1967; Laguta *et al.*, 2016). For the anion type in the <D> site, fluoride garnets have also been reported in addition to oxide garnets (De Pape *et al.*, 1967). In addition, N atoms could partially substitute O atoms in the <D> site by joint substitution of Si^{4+}–N^{3-} for Al^{3+}–O^{2-} (Wang *et al.*, 2012; Asami *et al.*, 2019).

However, the quantitative relationship between the chemical composition and the garnet phase stability lacks investigation. For example, only $(Ca)_3\{Al\}_2[Si]_3<O>_{12}$ could be synthesized in the garnet phase among $(M)_3\{Al\}_2[Si]_3<O>_{12}$ (M = Ca, Sr and Ba). Piccinelli *et al.* (2009) found that $Ca_3Sc_2Si_3O_{12}$ and $Ca_3Y_2Si_3O_{12}$ were characterized by different crystal structures, as the former is a cubic garnet, while the latter is an orthorhombic compound. Many researchers have investigated the crystal chemistry of garnets with reference to chemical compositions. Novak & Gibbs (1971) constructed the structural stability field of silicate garnets using multiple linear regression analyses. Geller (1967) compiled and discussed the ionic site selection covering almost all the common garnets. Euler & Bruce (1965) performed least-squares refinement to locate O atoms and studied the effects of shortened shared edges on the shape of polyhedra. Locock (2008) programmed a spreadsheet to calculate the molar proportions of garnet end-members from chemical analysis. Nevertheless, until now, the direct link connecting chemical compositions and the garnet phase is still unknown.

The tolerance factor in perovskite structures was the inspiration to search for a stoichiometric parameter for the prediction and systematic description of the garnet structure. According to Langley & Sturgeon (1979) and Hawthorne (1981), multiple regression analyses of numerous garnet compounds reveal a systematic linear relationship between the lattice parameters/mean bond lengths and ionic radii. This favours the hard-sphere packing of ions in the garnet structure, which is also the basic assumption used in the derivation of the tolerance factor of the perovskite structure. In this work, the garnet-owned tolerance factor is introduced based on a geometrical analysis of the multipolyhedral constraints. During the calculation, only the ionic radius of the chemical species are needed. More than 130 garnet end-members have been surveyed for tolerance factors, which are located in a narrow range around 1. The results will be helpful in understanding and guiding the synthesis of novel garnet-type compounds.

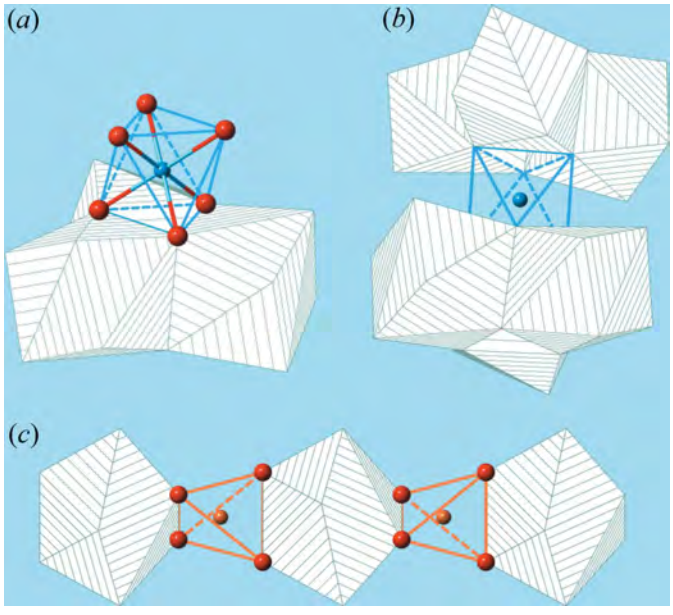

Figure 1
Connectivity between octahedron/tetrahedron and dodecahedron with sharing edges in the garnet structure. See §2.1 for details of what is shown in parts (*a*), (*b*) and (*c*).

2. Methods

2.1. Connectivity and modelling of the garnet structure

For the garnet structure, the connectivity between different polyhedra have been clarified concerning the corner- and edge-sharing types. Here, we mainly focus on the octahedron and tetrahedron sharing edges with the dodecahedron. In the garnet structure, three dodecahedra are combined *via* sharing edges into a triangular unit, which is docked to one face of the octahedron, as shown in Fig. 1(*a*). For that octahedron, the counterpart face is docked with the other dodecahedral triangular unit. In Fig. 1(*b*), the two dodecahedral triangular units are orientated with interlaced parts. Tetrahedra link dodecahedra *via* sharing edges in a rotational manner, as illustrated in Fig. 1(*c*). From the above analysis, it is noticeable that the packing of dodecahedra plays the main role in constituting the garnet structure, while octahedra and tetrahedra connect different parts of the dodecahedra. From this point of view, the ionic radii of the cations and anions from the chemical compositions have to fulfill the garnet structure compliance.

Furthermore, the garnet structure is simplified in order to obtain a vivid understanding of the doecahedral packing. The distorted dodecahedron reverts to a regular cube and the triangular unit now consists of three identical cubes, as shown in Fig. 2(*a*). In this model, the octahedron still connects the interlaced two triangular units. In order to reveal the tetrahedral link between dodecahedra, the triangular unit in

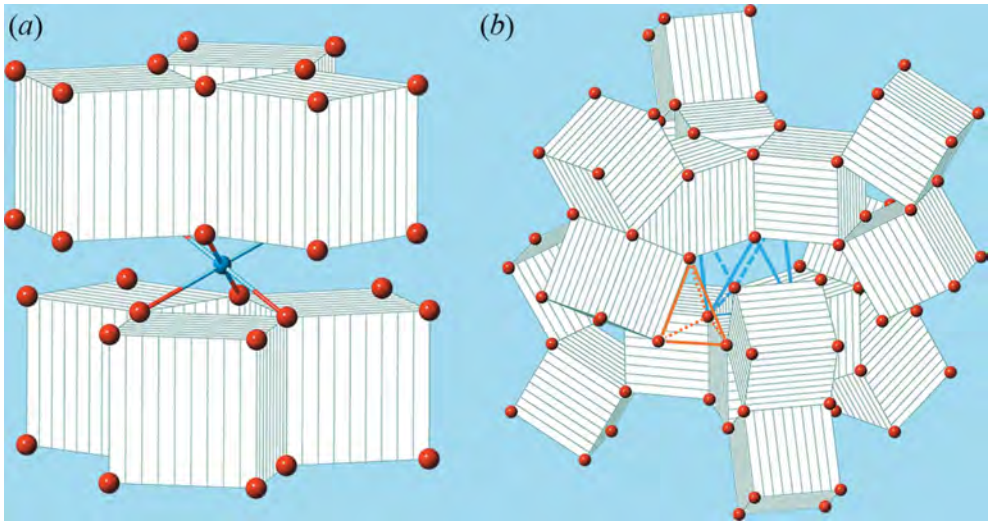

Figure 2
Modelling of the garnet structure. The distorted cubes are represented by regular ones in order to demonstrate how the polyhedra are packed and connected. See §2.1 for details of what is shown in parts (*a*) and (*b*).

Fig. 2(*a*) is further extended in Fig. 2(*b*). The orange one connecting the extension of the upper unit and the lower unit is denoted as the linking tetrahedron. Considering the geometrical relationships in this simplified model, we assign the distance between two neighbouring triangular units as the structural parameter, which equals the height of the tetrahedron (the orange one in Fig. 2*b*).

2.2. Expression for tolerance factor using ionic radius

With the basic geometrical relationship established, the tolerance factor of the garnet structure could be constructed supposing all the ions are close-packed (Fig. S1 in the supporting information). Let R_A, R_B, R_C and R_D stand for the radii of the ions occupying dodecahedron (A), octahedron{B}, tetrahedron [C] and general position <D>, respectively. When it comes to the simplified model, (A) corresponds to a regular cube and the edge length L has a relationship with the body diagonal length as

$$\sqrt{3}L = 2R_A + 2R_D.$$

The distance between neighbouring triangular units is related to L. As shown in Fig. 2(*b*), the upper cap of the octahedron is a regular triangle with edge length L. Its centre, the {B} ion and the <D> ion constitute a right-angled triangle. Therefore, the distance is calculated as

$$L' = 2\sqrt{(R_B + R_D)^2 - \left(\frac{\sqrt{3}}{3}L\right)^2}.$$

Meanwhile, by simple solid geometrical calculations, it is known that the height H of the tetrahedron with edge length L'' is

$$H = \sqrt{\frac{2}{3}}L'',$$

while

$$L'' = \sqrt{\frac{8}{3}}(R_C + R_D).$$

Finally, the tolerance factor, τ, is defined as the ratio between the distance L' and the tetrahedral height H,

$$\tau = \frac{L'}{H} = \frac{2\sqrt{(R_B + R_D)^2 - \left(\frac{\sqrt{3}}{3}L\right)^2}}{\sqrt{\frac{2}{3}} \times \sqrt{\frac{8}{3}}(R_C + R_D)} = \frac{3\sqrt{(R_B + R_D)^2 - \frac{4}{9}(R_A - R_D)^2}}{2(R_C + R_D)}.$$

The ionic radius of all the chemical species constituting the garnet structure are included in τ. For real garnet-based compounds, the value of τ is expected to fluctuate around 1, and the numerical limits could be identified by non-existent garnet phases.

3. Results and discussion

3.1. Survey of garnet structures with different chemical compositions using the tolerance factor

In order to check the reliability of the tolerance factor, more than 130 real or hypothetical garnet-relevant compounds were surveyed. During the calculations, the Shannon ionic radii (Shannon, 1976) were selected in accordance with the coordination number, *i.e.* 8 for (A), 6 for {B}, 4 for [C] and 4 for <D>. The results are listed in Table S1 in the supporting information. The identification number is ascribed according to the chemical compositions. The first digit stands for the atomic number of elements in <D> sites, which is 8 for oxygen and 9 for fluorine. For the next six digits, every two successive ones represents the atomic number of elements in [C], {B} and

(A) sites, respectively. The last digit is zero for end-member garnets, *i.e.* the four crystallographic sites are solely occupied by only one type of chemical composition, and '1' for non-end-member garnets. Therefore, every garnet-type compound in Table S1 is numbered together with the reference proving the garnet phase existence, and the calculated τ values fill the last column of Table S1. Among all the numbered garnet-type compounds, only eight of them belong to fluoride garnets, whereas the remaining ones all have O atoms at the <D> position. In addition, almost all the compounds in this survey are end-member garnets. Garnet-type solid solutions between end-members, such as $(Y)_3\{Al\}_2[Al]_3<O>_{12}$ and $(Gd)_3\{Al\}_2[Al]_3<O>_{12}$, or $(Y)_3\{Al\}_2[Al]_3<O>_{12}$ and $(Y)_3\{Ga\}_2[Ga]_3<O>_{12}$, are excluded in this survey for simplification, because their τ values just reside between those of end-members. The only exception is No. 83212391, *i.e.* $(Mg_{1/3}Y_{2/3})_3\{Mg\}_2[Ge]_3<O>_{12}$, which will be compared to the hypothetical No. 83239120, *i.e.* $(Mg)_3\{Y\}_2[Ge]_3<O>_{12}$, in the following section. The data for τ are then plotted for all the numbered compounds in Fig. 3, with the nongarnet phases denoted by crossed red circles, which will be discussed in detail. A quick view of Fig. 3 shows that the tolerance factor introduced in this work is reliable in indicating the garnet-phase formation from the given chemical compositions. The τ values for fluoride garnets range from 0.6 to 1.03. However, the range may be expanded with further reports of new fluoride garnets. More attention is paid to the oxide garnets, because the τ values of over 100 different chemical compositions are scattered in the range from 0.748 to 1.333. Just like the tolerance factor of the perovskite structure, the tolerance factor in the garnet structure also originates from the geometrical close-packing of compositional ions, and only the ionic radius is needed in evaluating the τ value. Next, the crystal chemistry and phase stability of selected garnet-type compounds will be discussed by means of the tolerance factor.

3.2. Crystal chemistry of garnet compounds from the point of view of the tolerance factor

The data points in Fig. 3 could be coarsely categorized with regard to the chemical composition in the [C] site. The data spread range seems related to the valence state of [C], since silicate and germanium garnets have a much wider range to that of aluminium, gallium and iron garnets. The possible explanation lies in the element choice under valence constraint. For $[C]^{4+}$, the valence scheme is $(A)^{2+}+\{B\}^{3+}$, whereas for $[C]^{3+}$, only cations with the +3 valence state are available for (A) and {B}. Consequently, there exist more compounds in $[C]^{4+}$-series garnets. Besides, the τ values for fluoride garnets are distributed in lower positions than those of oxide garnets in Fig. 3, which results from the smaller ionic radius of F^- compared to O^{2-}. It is known from the definition that the tolerance factor is defined on the basis of close packing of hard spheres, which assumes a larger anion volumetric occupation than that of the cation. As a result, the polyhedral shrinkage of {B} is more severe than that of [C], which leads to smaller τ values.

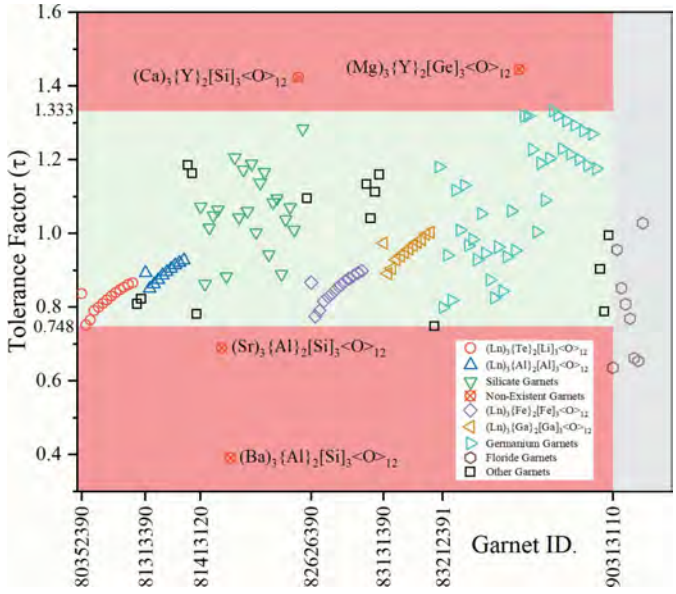

Figure 3
Survey of the tolerance factor (τ) of garnet-type compounds. The crossed red circles denote nongarnet phases.

3.2.1. Silicate–aluminium garnets containing alkaline earth metal elements (Nos. 81413200, 81413380 and 81413560). In silicate–aluminium garnets containing alkaline earth metal elements, $(M)_3\{Al\}_2[Si]_3<O>_{12}$ (M = Ca, Sr and Ba for Nos. 81413200, 81413380 and 81413560, respectively), the Ca-garnet has been widely reported (Ottonello *et al.*, 1996; Geiger & Armbruster, 1997; Meagher, 1975; Pkandl, 1966; Sawada, 1999). It has a τ value of 0.863, whereas the Sr- and Ba-garnets have much smaller τ values, *i.e.* 0.690 and 0.391, respectively. The trend stems from the increasing ionic radius, R_A, in the sequence $R_{Ca} < R_{Sr} < R_{Ba}$. With reference to Fig. 2, this implies that the [Si] tetrahedra are unable to connect neighbouring dodecahedral triangular units. Therefore, from the viewpoint of the tolerance factor, $(Sr)_3\{Al\}_2[Si]_3<O>_{12}$ and $(Ba)_3\{Al\}_2[Si]_3<O>_{12}$ can hardly form the garnet phase. This is confirmed by the failure to synthesize garnets of these compositions, as reported by Gentile & Roy (1960). Meanwhile, Novak & Gibbs (1971) also gave explanations based on the anomalous features in the structural stability of the hypothetical silicate garnets structures. Nevertheless, Sr-garnets are discovered in germanium garnets, such as $(Sr)_3\{Y\}_2[Ge]_3<O>_{12}$ (Marin *et al.*, 1991; Pasiński & Sokolnicki, 2017) (No.83239380, τ = 1.228).

3.2.2. Silicate–yttrium garnets containing metal elements with the valence state +3 (No. 814XX200). Silicate–yttrium garnets containing metal elements with the valence state +3 (No. 814XX200) share the formula $(Ca)_3\{M\}_2[Si]_3<O>_{12}$, in which M stands for metal elements with the valence state +3. Transition-metal elements from the fourth period contribute most to {M}. On increasing the ionic radius of {M}, $(Ca)_3\{In\}_2[Si]_3<O>_{12}$ is reported to form in the garnet phase (No. 81449200, τ = 1.285) (Novak & Gibbs, 1971; Li *et al.*, 2010), but $(Ca)_3\{Y\}_2[Si]_3<O>_{12}$ crystallized in an orthorhombic structure (No. 81439200, τ = 1.423) (Piccinelli *et al.*, 2009; Yamane *et al.*, 1997). On the contrary, when [Si] is substituted

for larger [Ge], $(Ca)_3\{Y\}_2[Ge]_3<O>_{12}$ has the garnet phase (No. 83239200), with a smaller τ value of 1.319. The reason may lie in the fact that larger [Ge] increases the tetrahedral size to connect the neighbouring dodecahedral triangular units.

3.2.3. Cation distribution in inverse garnet $Mg_3Y_2Ge_3O_{12}$. The tolerance factor could be used to interpret the cation distribution in inverse garnet $Mg_3Y_2Ge_3O_{12}$. The nomenclature for inverse garnet is used with analogy to normal and inverse spinels (Lévy & Barbier, 1999). By comparison with $(Ca)_3\{Y\}_2[Ge]_3<O>_{12}$, it seems that in the composition of $Mg_3Y_2Ge_3O_{12}$, larger Y^{3+} occupies the octahedral site, while smaller Mg^{2+} is accommodated in the dodecahedral site (No. 83239120, hypothetical). However, this cation distribution scheme gives τ values as high as 1.445, far beyond the normal range of the tolerance factor. Lévy & Barbier (1999) had discovered a mixed Mg^{2+}/Y^{3+} occupancy of the dodecahedral site, with the crystal formula $(Mg_{1/3}Y_{2/3})_3\{Mg\}_2[Ge]_3<O>_{12}$. This scheme lowers the τ value to 1.181, which is more reasonable for the garnet phase.

Lanthanide garnets constitute a large part of the garnet series and they have a relatively narrow data spread due to the consecutive decrease in ionic radius for rare-earth elements. Generally, lanthanide elements tend to occupy (A) and {B} sites. In the first case, the tolerance factors increase throughout the lanthanide series, as in the $(Ln)_3\{Al\}_2[Al]_3<O>_{12}$, $(Ln)_3\{Ga\}_2[Ga]_3<O>_{12}$ and $(Ln)_3\{Fe\}_2[Fe]_3<O>_{12}$ series. On the other hand, in the $(Ca)_3\{Ln\}_2[Ge]_3<O>_{12}$ series, where lanthanide elements are accommodated in the octahedral sites, the tolerance factor decreases.

4. Conclusion

The tolerance factor introduced is expected to serve as a useful structural descriptor for the garnet structure. Thus, the crystal chemistry, phase stability and material properties of garnet-type compounds could be investigated to a deeper level. Chemists and materials researchers could further employ the tolerance factor in machine learning and high-throughput screening applications to discover new compounds with the garnet structure.

Funding information

Funding for this research was provided by: National Natural Science Foundation of China (grant Nos. 51832005 and 51602019).

References

Asami, K., Ueda, J., Shiraiwa, M., Fujii, K., Yashima, M. & Tanabe, S. (2019). *Opt. Mater.* **87**, 117–121.
Bachmann, V., Ronda, C. & Meijerink, A. (2009). *Chem. Mater.* **21**, 2077–2084.
Bartel, C. J., Sutton, C., Goldsmith, B. R., Ouyang, R., Musgrave, C. B., Ghiringhelli, L. M. & Scheffler, M. (2019). *Sci. Adv.* **5**, No. 2, eaav0693.
Cao, Y., Wang, N., Tian, H., Guo, J., Wei, Y., Chen, H., Miao, Y., Zou, W., Pan, K., He, Y., Cao, H., Ke, Y., Xu, M., Wang, Y., Yang, M., Du, K., Fu, Z., Kong, D., Dai, D., Jin, Y., Li, G., Li, H., Peng, Q., Wang, J. & Huang, W. (2018). *Nature*, **562**, 249–253.
Chen, Q., Wu, J., Ou, X., Huang, B., Almutlaq, J., Zhumekenov, A. A., Guan, X., Han, S., Liang, L., Yi, Z., Li, J., Xie, X., Wang, Y., Li, Y., Fan, D., Teh, D. B. L., All, A. H., Mohammed, O. F., Bakr, O. M., Wu, T., Bettinelli, M., Yang, H., Huang, W. & Liu, X. (2018). *Nature*, **561**, 88–93.
De Pape, R., Portier, J., Gauthier, G. & Hagenmuller, P. (1967). *C. R. Acad. Sci. Paris Ser. C*, **265**, 1244–1246.
Euler, F. & Bruce, J. A. (1965). *Acta Cryst.* **19**, 971–978.
Geiger, C. A. & Armbruster, T. (1997). *Am. Mineral.* **82**, 740–747.
Geller, S. (1967). *Z. Kristallogr. Cryst. Mater.* **125**, 1–47.
Gentile, A. & Roy, R. (1960). *Am. Mineral. J. Earth Planet. Mater.* **45**, 701–711.
Goldschmidt, V. M. (1926). *Naturwissenschaften*, **14**, 477–485.
Green, M. A., Ho-Baillie, A. & Snaith, H. J. (2014). *Nat. Photon.* **8**, 506–514.
Grinberg, I., West, D. V., Torres, M., Gou, G., Stein, D. M., Wu, L., Chen, G., Gallo, E. M., Akbashev, A. R., Davies, P. K., Spanier, J. E. & Rappe, A. M. (2013). *Nature*, **503**, 509–512.
Hawthorne, F. C. (1981). *J. Solid State Chem.* **37**, 157–164.
Itoh, M., Wang, R., Inaguma, Y., Yamaguchi, T., Shan, Y.-J. & Nakamura, T. (1999). *Phys. Rev. Lett.* **82**, 3540–3543.
Kieslich, G., Sun, S. & Cheetham, A. K. (2015). *Chem. Sci.* **6**, 3430–3433.
Laguta, V., Zorenko, Y., Gorbenko, V., Iskaliyeva, A., Zagorodniy, Y., Sidletskiy, O., Bilski, P., Twardak, A. & Nikl, M. (2016). *J. Phys. Chem. C*, **120**, 24400–24408.
Langley, R. H. & Sturgeon, G. D. (1979). *J. Solid State Chem.* **30**, 79–82.
Lévy, D. & Barbier, J. (1999). *Acta Cryst.* C**55**, 1611–1614.
Li, H.-L., Kuang, X.-Y., Mao, A.-J., Li, Y. & Wang, S.-J. (2010). *Chem. Phys. Lett.* **484**, 387–391.
Li, Y., Chen, X., Dolocan, A., Cui, Z., Xin, S., Xue, L., Xu, H., Park, K. & Goodenough, J. B. (2018). *J. Am. Chem. Soc.* **140**, 6448–6455.
Lin, K., Xing, J., Quan, L. N., de Arquer, F. P. G., Gong, X., Lu, J., Xie, L., Zhao, W., Zhang, D., Yan, C., Li, W., Liu, X., Lu, Y., Kirman, J., Sargent, E. H., Xiong, Q. & Wei, Z. (2018). *Nature*, **562**, 245–248.
Locock, A. J. (2008). *Comput. Geosci.* **34**, 1769–1780.
Lu, J., Ueda, K., Yagi, H., Yanagitani, T., Akiyama, Y. & Kaminskii, A. (2002). *J. Alloys Compd.* **341**, 220–225.
Marin, S. J., O'Keeffe, M., Young, V. G. & Von Dreele, R. B. (1991). *J. Solid State Chem.* **91**, 173–175.
Meagher, E. (1975). *Am. Mineral. J. Earth Planet. Mater.* **60**, 218–228.
Menzer, G. (1929). *Z. Kristallogr. Cryst. Mater.* **69**, 300–396.
Muñoz-García, A. B., Artacho, E. & Seijo, L. (2009). *Phys. Rev. B*, **80**, 014105.
Muñoz-García, A. B., Barandiarán, Z. & Seijo, L. (2012). *J. Mater. Chem.* **22**, 19888–19897.
Novak, G. A. & Gibbs, G. V. (1971). *Am. Mineral. J. Earth Planet. Mater.* **56**, 791–825.
Ottonello, G., Bokreta, M. & Sciuto, P. F. (1996). *Am. Mineral.* **81**, 429–447.
Pasiński, D. & Sokolnicki, J. (2017). *J. Alloys Compd.* **695**, 1160–1165.
Piccinelli, F., Speghini, A., Mariotto, G., Bovo, L. & Bettinelli, M. (2009). *J. Rare Earths*, **27**, 555–559.
Pkandl, W. (1966). *Z. Kristallogr. Cryst. Mater.* **123**, 81–116.
Saliba, M., Matsui, T., Domanski, K., Seo, J.-Y., Ummadisingu, A., Zakeeruddin, S. M., Correa-Baena, J.-P., Tress, W. R., Abate, A., Hagfeldt, A. & Grätzel, M. (2016). *Science*, **354**, 206–209.
Sawada, H. (1999). *J. Solid State Chem.* **142**, 273–278.
Shannon, R. D. (1976). *Acta Cryst.* A**32**, 751–767.
Song, Z., Xia, Z. G. & Liu, Q. L. (2018). *J. Phys. Chem. C*, **122**, 3567–3574.
Wang, X., Zhao, Z., Wu, Q., Li, Y. & Wang, Y. (2016). *Inorg. Chem.* **55**, 11072–11077.

Wang, X., Zhou, G., Zhang, H., Li, H., Zhang, Z. & Sun, Z. (2012). *J. Alloys Compd.* **519**, 149–155.
Xia, Z. G. & Meijerink, A. (2017). *Chem. Soc. Rev.* **46**, 275–299.
Xu, J., Murata, D., So, B., Asami, K., Ueda, J., Heo, J. & Tanabe, S. (2018). *J. Mater. Chem. C,* **6**, 11374–11383.
Yamane, H., Nagasawa, T., Shimada, M. & Endo, T. (1997). *Acta Cryst.* C**53**, 1367–1369.
Zhang, N., Long, X., Wang, Z., Yu, P., Han, F., Fu, J., Ren, G., Wu, Y., Zheng, S., Huang, W., Wang, C., Li, H. & Liu, X. (2018). *ACS Appl. Energ. Mater.* **1**, 5968–5976.